Mausam, (1996), 47, 1, 1-20

551. 551.2 : 551.501.79

A semi-implicit multiple-nested grid model for simulation of flow in a tropical storm

J. C. MANDAL
Regional Meteorological Centre, Calcutta
(Received 28 April 1992, Modified 23 March 1995)

सार — उष्णकटिबंधीय चक्रवात के अनुरूपण के लिए अनुकूल, एक तीन-स्तरीय त्रिआयामी त्रिविमीय (ट्रिपली नेस्टेड) ज्ञाच समीकरण निदर्श का अभिकल्पन किया गया है। इसमें एक ग्रिड टेलीस्कोपी तकनीक का प्रयोग किया गया है, जिसमें केन्द्र में 18 कि० मी० ग्रिड लम्बाई की एक उत्तम ग्रिड जाली है जो 54 कि० मी० ग्रिड लम्बाई की मध्यम जाली से घिरी है और इसके चारों ओर एक 162 कि० मी० की ग्रिड लम्बाई की मोटी जाली और लगाई गई है। प्रत्येक जाली में संवेग बिंदुओं के 32 × 32 व्यूह हैं जिसमें 31 × 31 व्यूह संहति बिंदुओं के हैं। परिवर्तिताओं को रिक्त स्थान में अंतरित किया गया जिससे औसत मात्रा न्यूनतम हो जाती है और इस प्रकार से परिशुद्धि में सुधार होता है। अरैखिक अस्थिरता को कम करने के लिए विकसित, सीमित विभेद योजना उपयोग में लाई गई है। भिन्न लम्बाई की जालियों के बीच तालमेल हेतु एकद्विमार्गीय पारस्परिक क्रिया पद्धति अपनाई गई है। समाकलन के लिए समय सीमा बढ़ाने हेतु एक अर्ध-अव्यक्त योजना का उपयोग किया गया है। एक परस्पर प्रभावशाली पद्धति के प्रयोग से अर्धअव्यक्त योजना से उत्पन्न हेल्म्होल्टज समीकरण के समाधान की गति पर्याप्त मात्रा में बढ़ी है। सतह घर्षण की भूमिका का पता लगाने के लिए यामस्की (1977) द्वारा अभिग्रहित तथा आरनोल्ड (1977) द्वारा परिकल्पित बलित अवतलन की जांच की गई। भूमध्यसागरीय चक्रवात के विकास की प्रारम्भिक अवस्था से संबंधित ग्रे (1977) तथा यनाई (1961) के आधार पर इस निदर्श के बारे में संख्यात्मक प्रयोग पूरे किए गए जिसमें सतह-कर्षण के भिन्न गुणांकों पर चर्चा की गई जिसमें हैरिसन (1973) द्वारा प्रयुक्त की गई प्रणाली के समान विश्लेषणात्मक प्रणाली के माध्यम से विक्षोभ केन्द्र के आसपास ऊष्मा के बारे में बताया गया है जिसका कारण बलित अवतलन का प्रभाव माना गया है। समाकलन अनुप्रवण संतुलन में कम दाब घनत्वीय भ्रमिल से आरम्भ किया गया जो दो मामलों में 48 घंटे तक तथा एक मामले में 60 घंटे तक चलता रहा। इस बात का पता चला है कि जब भ्रमिल दुर्बल हो तब भूमध्यसागरीय चक्रवात की आरम्भिक अवस्था में विकसित होने का सतह-घर्षण आवश्यक कारण नहीं है। दूसरी तरफ इस बात का भी पता चला है कि बलित अवतलन भी चक्रवात के प्रारम्भिक विकास का कारण हो सकता है। परन्तु बाद की अवस्था में परिसीमा स्तर में बड़े पैमाने पर अभिसरण को प्रेरित करने में सतह-घर्षण महत्वपूर्ण भूमिका निभाता है तथा विक्षोभ के क्षैतिज पैमाने को कम करता है। इस प्रारम्भिक प्रयोग से अच्छे एवं उत्साहजनक परिणाम निकले हैं।

ABSTRACT. A three-layer three-dimensional, triply-nested primitive equation model, suitable to simulate tropical storm, has been designed. A grid telescopic technique has been used with a fine grid mesh of 18 km grid length in the centre which is surrounded by a medium mesh of 54 km grid length; this is again surrounded by a course grid mesh of 162 km grid length. Each mesh consists of 32 × 32 array of momentum points enclosing 31 × 31 array of mass points. The variables are staggered in space which reduces the amount of averaging to a minimum and hence improves accuracy. To suppress non-linear instability an improved finite difference scheme has been applied. A two-way interaction method has been adopted to match the solutions between grids of different lengths. To increase the time step for integration, a semi-implicit scheme has been used. The speed of the solution of the system of Helmholtz equations arising out of semi-implicit scheme has been appreciably increased by devising an iterative method. To examine the role of surface friction as postulated by Yamasaki (1977) and forced subsidence as hypothesized by Arnold (1977), Gray (1977) and Yanai (1961) at the initial stage of development of a tropical storm, numerical experiments have been accomplished with this model varying coefficient of surface drag, and specifying heat around the centre of the disturbance which is considered as the effect of forced subsidence through an analytical function similar to one used by Harrison (1973). The integration was started from a weak barotropic vortex in gradient balance and continued for 48 hous in two cases and 60 hours in one case. It is observed that surface friction may not be an essential factor at the initial stage of development of tropical storm when the vortex is weak. On the other hand, initial development could be initiated by forced subsidence. But in the subsequent stage, surface friction plays an important role to induce mass convergence in the boundary layer and to reduce horizontal scale of the disturbance. This preliminary experiment has yielded smooth and encouraging results.

Key words — Simulation, Tropical storm, Multi-nested, Equation of motion, Semi-implicit.

1. Introduction

Inspite of the fact that necessary climatological and geographical conditions for the formation of tropical storm prevail over large areas of the earth during storm seasons, actual appearance of storms is a relatively rare phenomenon. According to statistics, only about 80 tropical storms with maximum sustained wind 40-50 kt are observed per year over the entire globe; of these, between one-half and two-third attain hurricane strength. This indicates that there must be a rare coincidence of circumstances before development of a storm. On the other hand, experience has shown that once a

tropical storm is formed, it is a persistent phenomenon as long as it remains over the water of storm region. Very little is yet known about detailed mechanism of its incipient stage of development. The formation always occurs in connection with some kind of pre-existing disturbance associated with a deep cloud layer. All of these disturbances do not intensify into tropical storm. Only a small percentage of these systems starts intensifying. Numerous studies have been made to clarify the process of their formation; but no general mechanism has yet been accepted. The appearance of an upper level (500-200 hPa) warm area during its formation is commonly observed.

Palmen (1948) has pointed out that the extremely low sea level pressure in the centre of a fully developed tropical storm far exceeds the values that could be caused by hydrostatic effect of the temperature rise in the central cloud-free area due to release of latent heat of condensation.

The rate of change of temperature at a point is determined by horizontal advection and diffusion, vertical motion and diabatic heating. Horizontal advection and diffusion cannot produce the relative maximum in temperature associated with tropical storm with hurricane intensity; so a warm core must be produced either by warming associated with subsidence or excess of latent heating over adiabatic cooling.

Since heating due to liberation of latent heat of condensation at a point does not necessarily produce a temperature increase at the same point, there has been some controversy regarding the physical processes that are responsible for tropospheric warming necessary to produce a tropical storm of hurricane strength from a weak disturbance.

Gray (1977) states that direct cumulus cloud induced enthalpy change due to condensation processes is probably too small to explain increase needed for initial storm genesis and intensification. Condensation energy is almost wholly expended in supporting the cluster's vertical motion. The magnitude of this energy appears not to be fundamental potential for transformation to a storm. The various types of CISK (Conditional Instability of Second Kind) parametrization are directly linked with the amount of frictional convergence in the boundary layer. These are not likely very relevant to pre-storm disturbance maintenance and intensification.

Arnold (1977) and Gray (1977) have observed that low level circulation centres of growing cloud clusters are often found outside the convective regions. They hypothesize that the upper tropospheric outflow from the cluster is blocked by the large scale flow and forced to subside. The subsidence warms the air and hydrostatically lowers the surface air pressure. This surface pressure fall is larger than that which could result from direct cumulus heating alone. Gray (1979) considers a dynamical forced subsidence to be a necessary requirement for the genesis. Yanai (1963) stated that weak absolute vorticity at upper levels together with warming of middle tropospheric air is an almost necessary and sufficient condition for the development of a wave disturbance into typhoon. He noted that superposition of an upper level anticyclone and middle level warming might not be completely independent phenomena.

Yamasaki (1977) demonstrated that surface friction is not important at the early stage of development of tropical storm when its vorticity is not large. With a two-dimensional model, he has shown that (*i*) a disturbance may develop even when surface friction does not exist, and (*ii*) surface friction is one of the important factors to determine the horizontal scale of the disturbance. He also pointed out that it is uncertain whether a CISK mode exists in the actual atmosphere. Surface friction may be important to make the atmosphere humid by causing weak but long-lasting frictional convergence associated with the vorticity field of pre-existing large scale disturbance or basic shear flow.

One of the objectives of this study is to make an attempt to understand the role of surface friction as pointed out by Yamasaki (1977) and the hypothesis of Arnold (1977), Gray (1977) and Yanai (1961) for the initial development of a tropical storm. For this purpose preliminary numerical experiments have been accomplished on a three-dimensional multi-nested grids varying coefficient of surface drag and imposing artificial heating through an analytical function considered as the effect of forced subsidence.

Filtered models do place a definite limit on the accuracy of forecast. The motion in the tropics, and particularly in tropical storm is essentially ageostrophic; hence, they can only be represented by the primitive equation. The primitive equation model, after elimination of acoustic wave propagation through incompressibility assumption, does include inertia-gravitational wave as the fastest moving mode as a solution. For this reason, the time steps in primitive equation forecast must be

considerably shorter than those allowed for filtered model with equal grid length, as it has no gravity wave solution, and depends upon the maximum wind speed and grid length. Although, the use of an implicit method removes the dependence of the time step on grid length, it is difficult to apply it to a non-linear system of equations. Also, there is undesirable damping of physical modes in many implicit schemes.

The numerical simulation of synoptic and mesoscale phenomena of the atmosphere, such as frontal wave, tropical storm etc. requires a grid with very small mesh size. Due to limitation of computing capacity and time, it is extremely difficult to fill the entire region with such a fine mesh and handle it. In order to overcome these difficulties a "nested grid" was first used by Hill (1968) for quasi-geostrophic model. The system consists of a limited fine mesh area in the region of interest embedded within a larger domain of coarse mesh. Multiple grids are also used stepwise so as to reduce the grid size less suddenly and are called the "telescopic grids".

One of the most crucial problems in nesting of grid is how to connect the solutions from various meshed grids. Matsuno (1966) and Browning *et al.* (1973) have found that wave motions in two unequal meshes have different phase speeds due to different truncation errors, and as a result numerical problem usually develops.

The application of multinested grid, in problems of tropical storm, has been presented by several authors, *e.g.*, for simulation of hurricane—Madala and Piases (1975) and Jones (1977), and for real data forecast — Mathur (1974), Ley and Elsberry (1976) and Ookochi (1978). These studies have provided with useful information and encouragement to the present study. In our limited area model, we have used triply-nested grids and semi-implicit scheme for time integration.

In semi-implicit scheme for integration, the time steps may be increased significantly. Robert *et al.* (1972) have extended this scheme to multilevel primitive equation model. Chen and Miyakoda (1974) have pointed out that in semi-implicit scheme the speed of integration is about four times faster than the leap-frog method for non-nested grid problem, and is about eight times faster than Euler's backward method of explicit scheme. For the nested grid calculation, this advantage is even greater.

But while adopting semi-implicit scheme, coupled Helmholtz equations for one of the appropriate variables are to be solved for each layer at each time step offsetting some of the computer time savings achieved by larger time step. To retain the advantage of this technique, an efficient method is necessary to solve the Helmholtz equations. The commonly used iterative method such as successive over relaxation (SOR) is fast for diagonally dominant equations; however, it converges slowly or may even diverge for weekly or non-diagonally dominant equations. In SOR method the optimal value of the over-relaxation coefficient depends on the number of grid points, specific form of the coefficients of the equation and error distribution. A theoretical estimate may be made only for a simplified form of equation. As such, one must resort to a sort of trial and error method to determine it (Sturat and O'Neill 1967).

The coefficient matrix of the Helmholtz equations obtained in this study is not symmetric or diagonally dominant at each level. Moreover, the equations are coupled among levels. So to solve these equations, we first used Stabilized Error Vector Propagation (SEVP) method (Madala 1978), an efficient direct solver. Simultaneously, we haunted for other efficient technique, and ultimately have developed an iterative method which we call "Simultaneous Multi-level Relaxation (SMR)"; as during iteration, improvements over the previous values on all levels for any particular horizontal grid point are made simultaneously. This method took lesser time than the SEVP method.

Other important purposes of the present study are to examine the computational reliability of the proposed multinested grid, advantage of the semi-implicit scheme, and also testing of the finite difference scheme for the non-linear terms.

2. Design of the model

The numerical model used in this study is a three-dimensional primitive equation model. It contains three layers in the vertical (Fig. 1). The lowest layer can be called the surface boundary layer; since, a major part of inflow in a tropical storm occurs in this layer. The top layer contains most of the upper troposphere which can be called the outflow layer as most of the outflow occurs in this layer. The middle layer is characterized by strong tangential velocities with no pronounced radial mass flux.

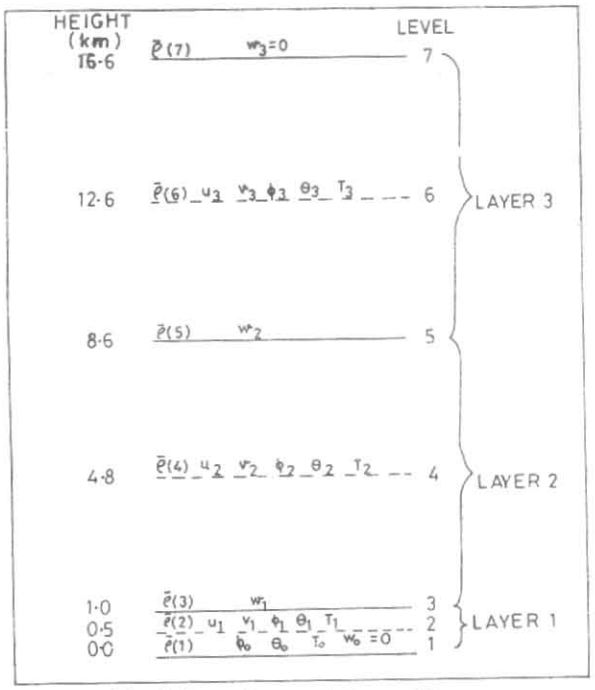

Fig. 1. Three layers of the model

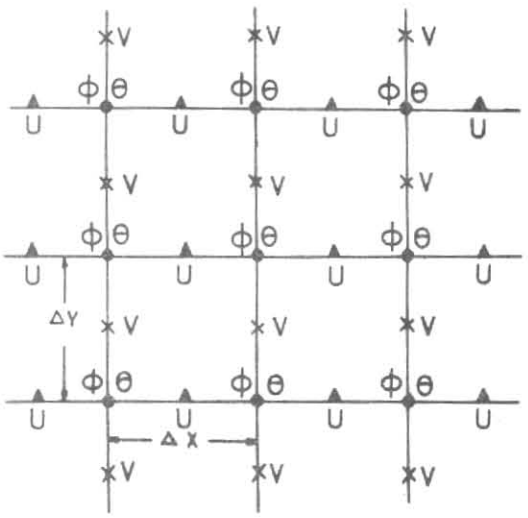

Fig. 2. Grid network in x-y plane

2.1. *Basic equations*

The basic equations on an *f*-plane ($f = 5 \times 10^{-5}\text{sec}^{-1}$) may be written in Cartesian co-ordinate system (c.f. Rosenthal 1969, Madala and Piacsek 1975) as follows :

$$\frac{\partial \bar{\rho} u}{\partial t} + \frac{\partial \bar{\rho} u^2}{\partial x} + \frac{\partial \bar{\rho} uv}{\partial y} + \frac{\partial \bar{\rho} uw}{\partial z} - f\bar{\rho}v$$

$$= -\bar{\rho}\theta \frac{\partial \Phi}{\partial x} + \frac{\partial \tau_{xx}}{\partial x} + \frac{\partial \tau_{yx}}{\partial y} + \frac{\partial \tau_{zx}}{\partial z} \qquad (1)$$

$$\frac{\partial \bar{\rho} v}{\partial t} + \frac{\partial \bar{\rho} uv}{\partial x} + \frac{\partial \bar{\rho} v^2}{\partial y} + \frac{\partial \bar{\rho} vw}{\partial z} + f\bar{\rho}u$$

$$= -\bar{\rho}\theta \frac{\partial \Phi}{\partial y} + \frac{\partial \tau_{xy}}{\partial x} + \frac{\partial \tau_{yy}}{\partial y} + \frac{\partial \tau_{zy}}{\partial z} \qquad (2)$$

$$\frac{\partial \Phi}{\partial z} = -\frac{g}{\theta} \qquad (3)$$

$$\frac{\partial \bar{\rho} u}{\partial x} + \frac{\partial \bar{\rho} v}{\partial y} + \frac{\partial \bar{\rho} w}{\partial z} = 0 \qquad (4)$$

$$\frac{\partial \bar{\rho}\theta}{\partial t} + \frac{\partial \bar{\rho} u\theta}{\partial x} + \frac{\partial \bar{\rho} v\theta}{\partial y} + \frac{\partial \bar{\rho} w\theta}{\partial z}$$

$$= \frac{\bar{\rho} H}{\Phi} + \frac{K_H}{\Phi} \bar{\rho} C_P \nabla^2_H \theta \qquad (5)$$

$$\theta\Phi = C_P T \qquad (6)$$

where, x, y, z and t are the independent space and time co-ordinate variables; u, v, and w are the eastward, northward and vertical velocity components respectively; f is the Coriolis parameter; 'g' is the acceleration of gravity; p is pressure, p_0 is a reference pressure and taken equal to 1000 hPa; $[\Phi = C_P\ (p/p_0)^{R/C_P}]$ is a new variable in place of pressure; C_P is specific heat of air at constant pressure ($=1004.64 \times 10^4$erg gm^{-1}deg^{-1}); R is specific gas constant of dry air ($=287.04 \times 10^4$erg gm^{-1}deg^{-1}); T is the air temperature; θ is the potential temperature; $\bar{\rho} = \bar{\rho}(z)$ is the density of mean tropical atmosphere which depends upon the vertical distance z only.

Eqns. (1) & (2) are the equations of motion in the east and north directions respectively. Since the horizontal dimension of a tropical storm is at least two orders of magnitude larger than the vertical dimension, the equation of motion for the vertical component of velocity can be simplified into the hydrostatic equation given by Eqn. (3). Eqn. (4) is a simplified form of the continuity equation that filters out acoustic wave solution (Ogura and Charney 1962; Ogura and Phillips 1962). Use of this form to simulate tropical storm can also be justified

by scale analysis. Eqn. (5) is the first law of thermodynamics. The first term 'H' on the right hand side of this equation represents diabatic heating (heat added or removed per unit mass of air per unit time). Vertical diffusion of heat is not included in the model because of relatively insufficient knowledge about the behavior of the vertical flux of heat in a tropical storm. Eqn. (6) is the relation among air temperature T, potential temperature θ and Φ. The terrain effect is excluded for simplicity.

We replace θ by $\alpha(\equiv 1/\theta)$, as α varies more linearly than θ between levels. For computational accuracy, we divide Φ and α into the basic (undisturbed) field (indicated by over bar) which is a function of z only and the perturbation part as below:

$$\Phi = \bar{\phi}(z) + \phi(x, y, z, t)$$

$$\alpha = \bar{\alpha}(z) + \alpha'(x, y, z, t) \qquad (7)$$

The horizontal and vertical momentum flux terms in the Eqn. (1) are assumed to be of the following form:

$$\tau_{xx} = \bar{\rho} K_H \frac{\partial u}{\partial x}, \tau_{yx} = \bar{\rho} K_H \frac{\partial u}{\partial y} \quad \tau_{zx} = \bar{\rho} K_Z \frac{\partial u}{\partial z};$$

and at the surface, we assume:

$$\tau_{zx} = \bar{\rho}(1) C_D u_1 \{u_1^2 + v_1^2\}^{1/2} \qquad (8)$$

with similar expression for τ_{xy}, τ_{yy} and τ_{zy} in Eqn. (2); where, K_H and K_Z are respectiveley the horizontal and vertical eddy coefficients of viscosity; C_D is drag coefficient; $\bar{\rho}(1)$ is the air density at the surface in the mean tropical atmosphere; u_1, and v_1, are the horizontal components of velocity at the 0.5 km level in the model.

We impose the following boundary condition on w:

$$w = 0 \text{ ; at } z = 0, \text{ and } z = Z_T.$$

where, Z_T denotes the upper boundary of the model atmosphere. When these conditions are imposed, external gravity waves are filtered out, because of the continuity Eqn. (4).

The sensible heat transfer between the tropical storm and the ocean surface is included implicitly in the model by assuming that the temperatures at levels 1 and 2 of the model (Fig. 1) are held constant for all time. This eliminates the need for a temperature forecast at levels 1 and 2 and for an explicit formulation of the air sea exchange of sensible heat. Frank (1977), in a composite study of hurricanes, showed that the boundary layer temperature is relatively constant with radius despite decreasing pressure towards the centre. Hawkins and Rubsam (1968) verified the isothermal expansion by estimating the surface temperatures of hurricane (Hilda 1964). The lifting condensation level of the surface air is assumed to be fixed for all time half way between levels 1 and 2 (500 m). The average specific humidity over the lowest 1 km is assumed to be the average saturation value for this layer. Above two assumptions eliminate the need for a water vapour convergence equation.

2.2. *Structure of the model*

McGregor and Leslie (1977) have shown that for semi-implicit schemes, the use of non-staggered grid with the usual time and space central finite difference approximations leads to a decoupling into four separate solutions on different elementary subgrids. A preferable procedure is to use a particular staggered grid which has no solution separation. This results in better treatment of geostrophic adjustment process and should predict the structure of small scale features more accurately. So, the variables in this model are specified in staggered grids (similar to Williams 1969), as shown in Figs. 2 and 3. The horizontal velocity components u and v are specified at levels 2, 4 and 6 (Fig. 1). The thermodynamic variables are specified at levels 1, 2, 4 and 6; the vertical velocity w is specified at levels 1, 3, 5 and 7. The pressure variable Φ and temperature variables T and θ which are defined at the same points form the basic grid. The velocity components u and v are defined at different points interlacing with the basic grid. The velocity points, u lie on the east-west Φ grid line at mid-way between its grid points; similarly, v points on north-south grid line. Finally, w points lie on the vertical lines through Φ points. Standard values of pressure, density, temperature and potential temperature in the mean tropical atmosphere at different levels of the model are given in Table 1.

The continuity equation is applied at a Φ point and is valid for the fluid unit surrounding that point. Through using an interlacing grid system, the amount of averaging reduces to a minimum; thus, improves accuracy. The continuity equation should have a unique exact form which can only be achieved by such a grid. This uniqueness is essential for deriving the Helmholtz equations in semi-

TABLE 1

Approximate values of pressure, temperature, potential temperature and density at various levels of the model in the mean tropical atmosphere (after Frank 1977)

Level	Height (km)	Pressure p (hPa)	Temperature T (°K)	Potential Temperature θ (°K)	Density $\bar{\varrho}$ (10^{-3} gm cm^{-3})
1	0.0	1010.000	299.700	298.850	1.17406
2	0.5	953.828	296.954	300.992	1.11902
3	1.0	900.030	294.201	303.164	1.06611
4	4.8	569.657	272.954	320.563	0.72708
5	8.6	346.571	249.454	337.659	0.48402
6	12..6	191.591	217.439	348.637	0.30697
7	16.6	97.982	190.321	369.600	0.17936

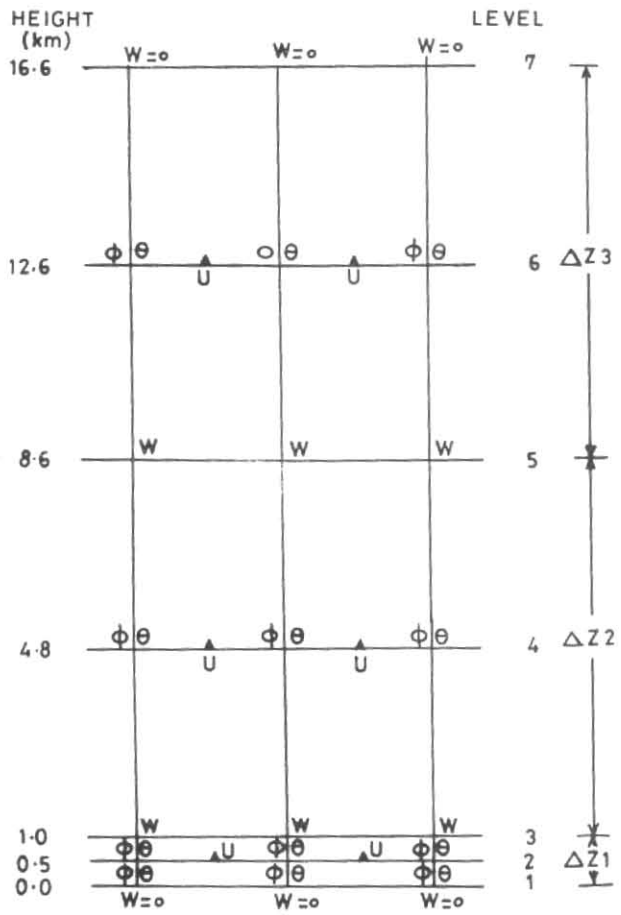

Fig. 3. Grid network in x-y plane

implicit scheme. To define Φ and T at the same point, is desirable for consistency with equation of state.

2.3. *Nested grids*

In a tropical storm, the dependent variables vary rapidly in the radial direction near the centre and less rapidly away from it. Therefore, a finer resolution of 10-20 km is required for representing the motion on the scale of a tropical storm '*eye*' and intensity forecast. But, it is not practically feasible to increase the spatial resolution throughout the entire domain. As such, a nested grid arrangement is considered suitable for this study. One important limitation is that the ratio of reduction of mesh should be such that certain coincident points are to be maintained between meshes for all the variables. In the staggered grid used in this model, minimum mesh ratio for adjacent grids must be 3 : 1. Considering all these points, we have used three nested meshes, each of uniform spacing. The innermost mesh with fine grid spacing of 18 km (hereafter called FG) is centered near the centre of the vortex. This is surrounded by a medium grid mesh (MG) with grid length of 54 km, which is again surrounded by another coarse grid mesh (CG) of 162 km grid length. Each mesh consists of 32 × 32 point array of momentum points enclosing 31 × 31 point array of mass points (Fig. 4).

3. Semi-implicit scheme and finite-difference equations

The semi-implicit method developed by Kwizak and Robert (1971) treats implicitly those terms in the equations of motion that are primarily responsible for the propagation of gravity waves. The

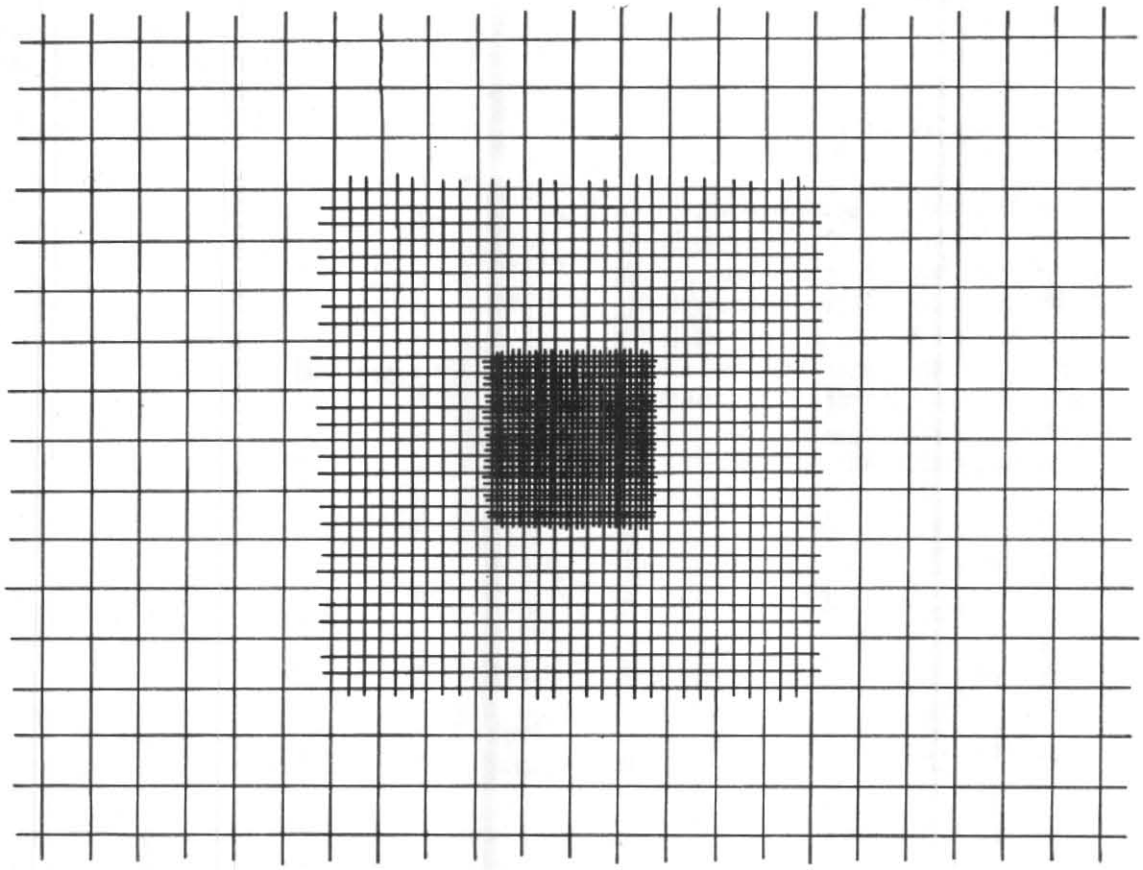

Fig. 4. The nested grid in x-y plane

advection terms are treated in an explicit fashion. The stability criteria for this method can be made to depend mainly upon the maximum wind speed and grid length, thus allowing longer time step. The time truncation errors associated with the permissible time step in semi-implicit method still remain an order of magnitude smaller than the errors associated with space truncation errors; and hence accuracy of the result is not lost. The way in which it is done, is to evaluate certain terms implicitly as a mean over times $(t-\Delta t)$ and $(t+\Delta t)$, rather than at time t. A coupled set of equations in time, then, results rather than a decoupled set. The method used in the present model is similar to the one described by Robert *et al.* (1972). Here the basic part of pressure gradient force, divergence and vertical advection of potential temperature are evaluated implicitly as a mean over times $(t-\Delta t)$ and $(t+\Delta t)$, and calculating all other terms of the variables at time t (Madala and Piàsek 1975).

3.1. *Finite difference operators*

To derive the finite-difference equations, the following sum and finite difference operators are used (vide Appendix A, for non-linear terms):

$$\bar{\beta}^{s} \equiv \frac{1}{2}\left[\beta\left(s+\frac{\Delta s}{2}\right)+\beta\left(s-\frac{\Delta s}{2}\right)\right]$$

$$\bar{\beta}^{2s} \equiv \frac{1}{2}\left[\beta(s+\Delta s)+\beta(s-\Delta s)\right]$$

$$\delta_s\beta \equiv \frac{1}{\Delta s}\left[\beta\left(s + \frac{\Delta s}{2}\right) - \beta\left(s - \frac{\Delta s}{2}\right)\right]$$

$$\delta_s^2 \equiv \delta_s(\delta_s\beta)$$

where, β represents one of the dependent variables u, v, w, Φ or α and s represents one of the independent variables x, y, z or t and Δs, the grid interval.

3.2. *Finite-difference equations*

Introducing the basic and perturbation parts in Φ and α as shown in the Eqn. (7), the terms in the Eqns. (1) to (5) are arranged in such a way that all terms on the left hand side will be treated implicitly using values at time $(t - \Delta t)$ and $(t + \Delta t)$; while the terms appearing on the right will be treated explicitly using the values at time t. Thus, the finite difference form of the above equations can be written in the following form (Mandal 1989):

$$\delta_t\overline{\bar{\rho}u}^t + \frac{\bar{\rho}}{\bar{\alpha}}\delta_x\bar{\phi}^{2t} = A_1 \tag{9}$$

$$\delta_t\overline{\bar{\rho}v}^t + \frac{\bar{\rho}}{\bar{\alpha}}\delta_y\bar{\phi}^{2t} = B_1 \tag{10}$$

$$\delta_z\bar{\phi}^{2t} = -\overline{g\bar{\alpha}'}^{2t} \tag{11}$$

$$\delta_x(\overline{\bar{\rho}u})^{2t} + \delta y(\overline{\bar{\rho}v})^{2t} + \delta_z(\overline{\bar{\rho}w})^{2t} = 0 \tag{12}$$

$$\delta_t(\overline{\bar{\rho}\alpha'})^t + \delta_z(\overline{\bar{\rho}w\bar{\alpha}})^{2t} = C_1 \tag{13}$$

where, the quantities A_1, B_1, and C_1 are functions of the dependent variables at time t, and will be evaluated first explicitly, and the implicit method will be applied to the remaining calculations.

The non-linearity in the equations of motion introduces computational instability from the finite difference approximation to the non-linear terms of the equations. Since, this instability results from the space truncation error of non-linear terms, it can not be eliminated either by reducing time step or by using implicit or semi-implicit method. One method is to suppress this instability by introducing artificial viscosity terms in finite difference equations. Grammeltvedt *et al.* (1969) showed that this can be controlled by devising a finite difference scheme for non-linear terms which satisfies certain linear and quadratic integral constraints. The finite difference form applied in this model conserves mass, momentum and total energy over a closed domain. In addition to these, difference equations approximately conserve mean square vorticity for non-divergent barotropic motion (Appendix A).

3.3. *Prediction equations*

The time averaged-set of prediction equations for u, v and α' from (9), (10), and (13) can be written as:

$$\overline{\bar{\rho}u}^{2t} + \frac{\bar{\rho}}{\bar{\alpha}}\Delta t\,\delta_x\bar{\phi}^{2t} = A \tag{14}$$

$$\overline{\bar{\rho}v}^{2t} + \frac{\bar{\rho}}{\bar{\alpha}}\Delta t\,\delta_y\bar{\phi}^{2t} = B \tag{15}$$

$$\overline{\bar{\rho}\alpha'}^{2t} + \Delta t\,\delta_z(\overline{\bar{\rho}w\bar{\alpha}})^{2t} = C \tag{16}$$

where,

$$A = A_1\Delta t + \bar{\rho}u(t - \Delta t)$$

$$B = B_1\Delta t + \bar{\rho}v(t - \Delta t)$$

$$C = C_1\Delta t + \bar{\rho}\alpha'(t - \Delta t)$$

Here, all terms on the right hand side of the above equations are known at time $(t - \Delta t)$ and t.

In order to determine $\bar{\phi}^{2t}$, the Eqns. (14) and (15) are differentiated with respect to x and y respectively and are added together. Then, eliminating the divergence part *via* continuity Eqn. (12), we get:

$$\frac{\bar{\rho}}{\bar{\alpha}}\Delta t\{\delta_x^2 + \delta_y^2\}\bar{\phi}^{2t} - \delta_z\overline{\bar{\rho}w}^{2t} = \delta_x A + \delta_y B \tag{17}$$

Applying hydrostatic Eqn. (11) to the three layers of the model and energy Eqn. (17) at the levels 4 and 6, $\overline{\bar{\rho}\alpha'}^{2t}$ can be eliminated to get $\overline{\bar{\rho}w}_1^{2t}$ and $\overline{\bar{\rho}w}_2^{2t}$ for the levels 3 and 5 respectively as:

$$\overline{\bar{\rho}w}_1^{2t} = FP1 \text{ and } \overline{\bar{\rho}w}_2^{2t} = FP2 \tag{18}$$

where, $FP1$ and $FP2$ are functions of $\bar{\phi}^{2t}$, grid lengths, time step, basic part of the variables and dependent variables at time $(t - \Delta t)$ and t.

Thereafter, applying Eqn. (17) at the levels 2, 4 and 6 and eliminating $\delta_z\overline{\bar{\rho}w}^{2t}$ the following set of

Elliptical (Helmholtz) equations in $\bar{\phi}^{2t}$ can be obtained.

$$\nabla_H^2\bar{\phi}_1^{2t}+a_{11}\bar{\phi}_1^{2t}+a_{12}\bar{\phi}_2^{2t}+a_{13}\bar{\phi}_3^{2t}=F_1 \quad (19)$$

$$\nabla_H^2\bar{\phi}_2^{2t}+a_{21}\bar{\phi}_1^{2t}+a_{22}\bar{\phi}_2^{2t}+a_{23}\bar{\phi}_3^{2t}=F_2 \quad (20)$$

$$\nabla_H^2\bar{\phi}_3^{2t}+a_{31}\bar{\phi}_1^{2t}+a_{32}\bar{\phi}_2^{2t}+a_{33}\bar{\phi}_3^{2t}=F_3 \quad (21)$$

where, ∇_H^2 represents horizontal Laplacian operator; the coefficients $a_{11}\ldots\ldots a_{33}$, are functions of the basic parts of thermodynamic variables, grid lengths and time step Δt; F_1, F_2, and F_3, are forcing functions computed explicitly at time t. For details, the readers are referred to Mandal (1989).

Having solved these equations for $\bar{\phi}_1^{2t}$, $\bar{\phi}_2^{2t}$ and $\bar{\phi}_3^{2t}$ by any direct or iterative method, the values of ϕ, u, v, w, and α' at time step $(t+\Delta t)$, can be calculated from the values of these variables at time $(t-\Delta t)$ using the implicit relation given below:

$$\chi(t+\Delta t)=2\bar{\chi}^{2t}-\chi(t-\Delta t) \quad (22)$$

where, χ represents any of the above variables.

The CFL stability condition of the type of grid used in the study is given by:

$$\Delta t \leqslant \Delta x\left[2(c^2+V^2)^{1/2}\right]^{-1}$$

where, Δt and Δx are the time and space increment; V is the maximum wind speed; and c is the phase speed of the fastest moving explicitly treated mode. It was considered prudent to use a conservative time step; so initially, a time step of 360 sec was used for all grids. Subsequently, it was reduced according to the stability criteria.

4. Computational procedure

4.1. *Solution of the system of Helmhotz equations*

In principle, it is possible to solve a system of Helmholtz equations by simultaneous relaxation method. Sela and Scolnik (1972) mentioned that this method is neither efficient nor elegant. They pointed out that by decoupling the efficiency becomes double. But their method of decoupling can not be adopted in this problem as the coefficient matrix is not symmetric.

As the system of Helmholtz Eqns. (19)-(21) are coupled in different levels, to apply the direct method, such as Error Vector Propagation method (EVP), each of the equations is required to be decoupled to an equation in a single dependent variable at each time step. The EVP method can not be applied in an area with large number of grid points. This has been overcome in the Stabilized Error Vector Propagation method (SEVP), a modification of EVP method, developed by Madala (1978) by dividing the integration region into blocks each of which is stable for EVP method. In the present problem this has been accomplished by dividing integration region of each mesh of 31 × 31 grid points into three overlapping blocks. In this (or other) direct method several subsidiary calculations are involved. Moreover, in the present problem the coefficient matrix is also not symmetric, so the transformation has been achieved by using latent vectors of the transpose of the coefficient matrix. After solving the new equations in terms of new variables independently of each other, they were again transformed back to the original set of variables by algebraic method. All these took sizable computer time and was not so easy for coding.

In the circumstances, we tried for other suitable method and have developed an iterative method (SMR) for such type of equations. It has been found that the total computer time required for a particular period of integration by this method is nearly two third of the time that required by SEVP method. In our method there is no need for decoupling the equations, easy to code and no extra memory is required as indirect method (Appendix B).

4.1.1 (a) *Divergence correction during integration*

In deriving the Helmholtz Eqns. (19)-(21), continuity equation has been used (Divergence = 0). If these equations could be solved exactly there was no problem. In reality, however, a degree of round-off error is inevitable even with trigonometric method. This, in turn creates an artificial divergence which can lead to computational instability.

By inserting round-off divergene at step $(t-\Delta t)$ as correction term in the forcing function for the solution for step $(t+\Delta t)$ (Williams 1969), it was found that divergence remained bounded.

4.2. *Boundary conditions and matching of the solutions*

This is a numerical model with a limited part of the atmosphere. One of the difficulties in this

connection is how to formulate the lateral boundary conditions on the outermost grid without imposing any physical constraint. To minimize the effect of the boundary conditions on the results, a square region with sides of 5184 km was selected for integration.

During the course of integration, all variables were held constant on the outermost grid boundaries. The spurious spatial oscillations were suppressed by applying a nine-point smoother (Shuman 1957) with smoothing element equal to 0.1 within four grids from the boundaries.

The most crucial problem in nesting of grids is how to connect the solutions of different grids. Various interface boundary conditions have been employed to permit mass, momentum and energy to flow between grids. But, no condition can be perfect, because of the differences in resolvable waves with different grid lengths (Elsberry 1979). In general, there are two approaches, *viz.*, one-way interaction and two-way interaction. In one-way interaction the boundary conditions for the fine mesh grid are specified from independent solutions of coarse grid area and there is no feed back from the fine grid to coarse grid solution. This results in unbounded growth unless controlled very carefully. In two-way interaction the solution for the fine mesh grid is obtained by using boundary conditions from coarse mesh grid and solution thus obtained in the fine mesh grid are substituted on common grid points of coarse mesh grid. Thus, the two mesh areas interact dynamically with each other. The scale interaction is more valid than reaction obtained with externally specified condition only. We have followed the second approach.

The computation proceeds from coarser grid to finer grid. First the forcing functions at all grid points are calculated. Then the diagnostic Eqns. (19)-(21) for $\bar{\phi}^{2t}$ are solved on the CG network. Boundary conditions of $\bar{\phi}^{2t}$ for the MG network are, then, obtained from CG solutions by four point cubic Lagrangian interpolation along the grid length followed by eighth order linear filter (Francis 1975) to remove two grid length irregularities. Initial guesses for MG mesh solutions are also obtained from CG data by similar interpolations from two orthogonal directions of the grids. This helps in reducing the number of iterations for both iterative and direct methods (in SEVP direct method, iterations are necessary to match the solutions of different blocks). Same procedure is repeated for the FG network. Having obtained the solutions for the three grid networks, at the common grid points between the FG and MG networks, the values of $\bar{\phi}^{2t}$ on the MG are replaced with the corresponding values obtained on the FG. Same process of back substitution is followed between MG and CG networks. The values of $\bar{\phi}^{2t}$ at the second row of MG and FG networks are smoothed by interpolation so that the second derivative normal to the grid boundary is equal to that derivative at third row.

Using the values of $\bar{\phi}^{2t}$ thus obtained, the values of u, v and α' can be calculated from the prognostic Eqns. (14)-(16); w from diagnostic Eqn. (18) and ϕ from implicit relation (22). Replacement of coarser grid values of all these variables by the finer grid data are done in the same way as in the preceding paragraph. The boundary values for u, v, w, and α' of the finer grid network are obtained by four point cubic Lagrangian interpolations of the coarser grid data. As on the finer grid along the eastern and western boundaries of u, and northern and southern boundaries of v, there is no coarser grid data, the interpolation is bi-cubic, *i.e.*, parallel and perpendicular to the interface. The values at the corner points are obtained as averages of values interpolated from two directions.

5. Numerical experiments

5.1. *Diabatic heating due to subsidence*

The amount and distribution of heat source due to subsidence is not well known in disturbance region. For this preliminary experiment, our approach is to test the effect of it with an analytical expression and see what can give better agreement between the model and observations. The horizontal heat distribution due to forced subsidence in the model atmosphere is formulated in a similar way as proposed by Harrison (1973). In actual tropical storm, one expects to find maximum heating at the centre of the storm. So, the horizontal heating function is given by:

$$Q = Q_0 \exp\left\{-\left(\frac{x-x_0}{r_0}\right)^2\right\} \exp\left\{-\left(\frac{y-y_0}{r_0}\right)^2\right\} \quad (23)$$

where, (x_0, y_0) is the horizontal location of the heating maximum, which is assumed to coincide with the centre of the storm; r_0 is the distance of the maximum tangential velocity from (x_0, y_0); Q is the amount of heat available in calorie per square centimeter per second to increase the air temperature of the layers 2 and 3, Q_0 being its maximum value.

Since the model predicts the temperature in layers 2 and 3 only, we assume that heat Q is distributed between these two layers in such a way that the amount of heat available to each layer is proportional to the difference of pseudo-adiabat (cloud temperature, T_c) and the temperature (T) of the storm scale circulation (Rosenthal 1969).

5.2. *Initial fields*

For this preliminary test, the time integration of the numerical model was started from a weak circularly symmetric, cyclonic vortex in gradient balance. The tangential wind, V_θ is of the following function of radius r.

$$V_\theta = V\max \left(\frac{r}{r_0}\right) \exp \frac{1}{2}\left[1-\left(\frac{r}{r_0}\right)^2\right] \qquad (24)$$

where, $V\max (= 9.8$ m/sec) is the maximum wind which is located at $r = r_0 (= 162$ km). Since the winds are constant in the vertical, the vortex is non-divergent and there is no radial or vertical motion. The choice of the initial vortex is of course to some degree arbitrary, as it is difficult to judge what should be the most realistic state. Sundquvist (1970) used the same form.

The gradient wind, after eliminating θ with the help of Eqn. (6), can be written as:

$$\frac{V_\theta^2}{r} + fV_\theta = C_P T \frac{\partial ln\Phi}{\partial r} \qquad (25)$$

This equation is solved for the distribution of Φ, by assuming that the temperature T is constant on any horizontal level and equal to the temperature of the mean tropical atmosphere at that level. The value of α, and hence, θ at any level is calculated from the hydrostatic equation.

5.3. *Surface friction*

In the concept of CISK mechanism to tropical cyclone theory, surface friction has been recognized as an essential factor for development of tropical storm. Yamasaki (1968), Ooyama (1969), Sundquvist (1970) and many other authors made numerical experiments on this concept. In their models, surface friction was indispensable to maintain the convective activity and disturbance should not develop when the drag coefficient concerning friction is reduced to zero. Linear analysis shows that the growth rate of tropical storm is directly proportional to the drag coefficient (Ooyama 1969). On the other hand, increased surface drag leads to an increased dissipation of kinetic energy. In Yamasaki's (1977) two dimensional model, it is found that large scale disturbance may develop, even if the surface friction is not taken into consideration.

Representation of the surface friction at the ground in terms of the large scale variables is a complex problem. In the conventional flux expressions, we need empirical determination of the drag coefficient C_D. Investigation in this context, have not yielded a conclusive relationship between C_D and wind. Some studies indicate a linear increase of C_D with increasing wind (Miller 1962); while according to Wu (1969), C_D becomes constant for sufficiently strong wind (greater than 15m/sec). Consequently, the numerical values of this coefficient include some uncertainty too.

5.4. *Three cases of the experiments*

The effect of the surface friction can be investigated by changing the value of C_D. In view of the discussions in the preceding section, following three numerical experiments have been performed to see how the surface friction and its variation can influence the development of a tropical storm in the early stage imposing artificial heating considered as the effect of forced subsidence.

Case A

Horizontal coefficient of eddy viscosity, K_H is taken equal to $10^4 m^2 sec^{-1}$; vertical coefficient, K_Z is $1\ m^2 sec^{-1}$ at level 2 and decreased linearly to zero at the top of the model; C_D is kept zero up to 20 hours, then linearly increased to 0.0025 from 20 hour to 40 hour and thereafter kept constant. The maximum diabatic heat, Q_0 is linearly increased from zero at the initial time to 68.8×10^{-3} calorie $cm^{-2}\ sec^{-1}$ at $t = 40$ hour; thereafter it is kept constant for the remaining time of integration. Equivalent amount in Harrison's (1973) model is much higher than this value.

Case B

The values of K_H, K_Z and C_D are zero during entire period of integration. Q_0 is linearly increased from zero at the initial time to 18.34×10^{-3} calorie $cm^{-2}\ sec^{-1}$ at 6 hour; thereafter it is kept constant for the remaining period of integration. This value is much smaller than that in case A.

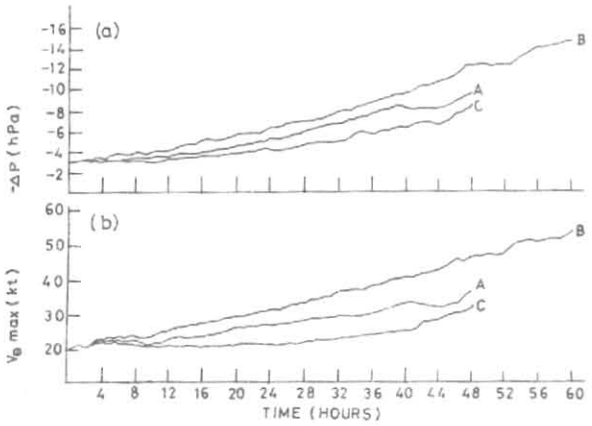

Figs. 5 (a & b). Time variation of (a) Central sea level pressure anomaly (hPa) and (b) Maximum wind at 0.5 km level (knots)

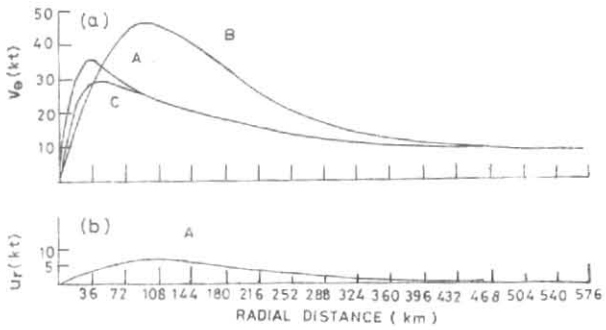

Figs. 6 (a &b). Mean tangential velocity (A, B, C), and (b) Radial winds (A) in knots

Case C

The values of K_H, K_Z and Q_0 are kept same as in Case A, but C_D is linearly increased from zero at the initial time to .0025 during a period of 40 hours, and thereafter kept constant.

6. Discussion of the numerical results

Since, the vortex in case A reached storm stage within 48 hours, and case C is similar type of A, the time integration of these two cases was discontinued after it. As the case B is frictionless, its integration was extended 12 hours more.

The time variations of central sea level pressure and the maximum winds at 0.5 km level in three cases are shown in Fig. 5. Though, there are small fluctuations on all curves throughout the time of integration, it is more pronounced on the velocity curves at the initial stage. Short period oscillations are not properly reflected as hourly data are plotted. Yamasaki (1977) mentioned that such oscillations are probably due to convective motion and gravity wave. Though the rate of diabatic heating in frictionless case is much smaller than other two cases, the rate of fall of central sea level pressure and increase of surface wind and their magnitudes are highest in this case. In C, the fall of central pressure or increase of surface wind upto 18 hours is very small. These are expected, since in B there is no dissipation of kinetic energy, and in C frictional term was included from the starting of integration. This figure indicates that at the termination of integration, the vortex was developing in all cases at a steady rate. In B, the central pressure has fallen from 1007 to 997.75 hPa in 60 hours; while in C, it fell from the same value to 1000.3 hPa in 48 hours. Starting from a weak vortex (19.8 kt), the system has intensified to a minimum storm (35 kt) at 30 hour in B, and at 47 hour in A; but in C, it could not attain this strength.

Radial variations of mean (around the centre) tangential velocity at 0.5 km level in three cases at 48-hour are shown in Fig. 6 (bottom). In B, the radius of the maximum tangential velocity is 100 km; while it is only 36 km in A and C. Such small values at this stage of development may be due to small radius (162 km) of the maximum velocity of the initial vortex. Radial gradient of diabatic heating may also have influence on this decrease. In B, the belt of high wind speed covers larger area than other two cases. In A and C, the speeds in the outer region are almost same; but around the radius of maximum wind, the profile of A has well defined peak, typical to real data; but in C, it is flat and its value is less than that in A, due probably to early imposition of C_D in C. These variations may be attributed to the variation of C_D. Radial variation of mean inflow velocity for A (Fig. 6, top) is smooth without any pronounced peak. Considering the early stage, this appears to be realistic. In C, it is of the same type; but in B, radial flow is very feeble.

Streamlines for the lower, middle (direction only) and upper (including isotach) levels in A at 48-hour are shown in Figs. 7 to 10. The streamlines clearly show that the flow is nearly symmetric at all levels. These are characterized by cyclonic inflow at the surface (Fig. 7) and outflow at the upper level

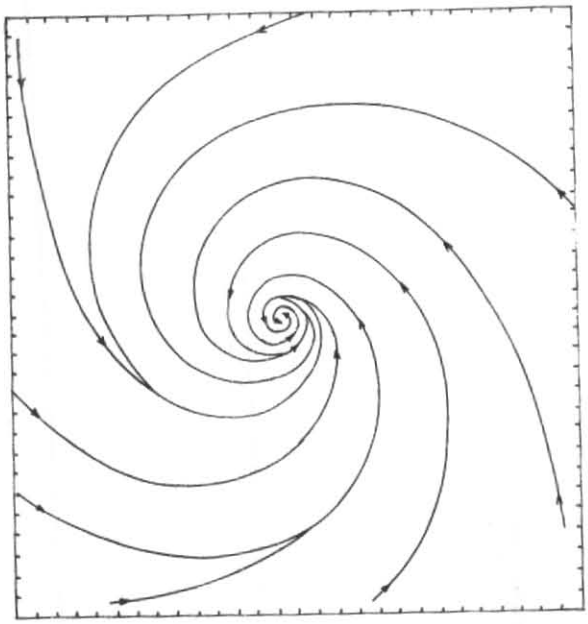

Fig. 7. Streamlines (A) of 0.5 km level at 48-hour, 18 km grid

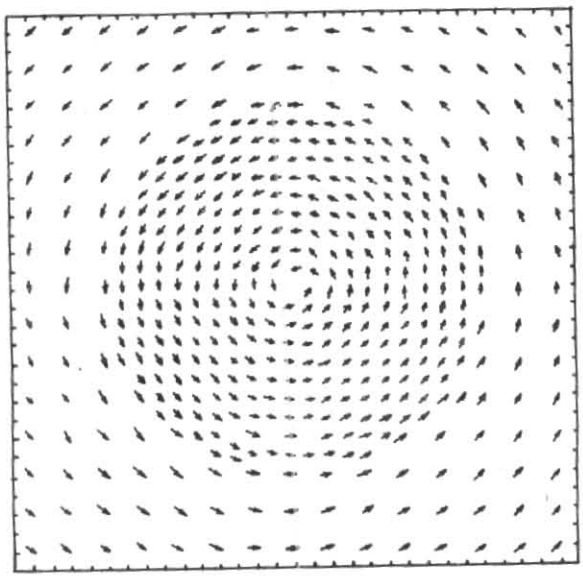

Fig. 8. Wind directions (A) of middle level at 48-hour, 18 km grid

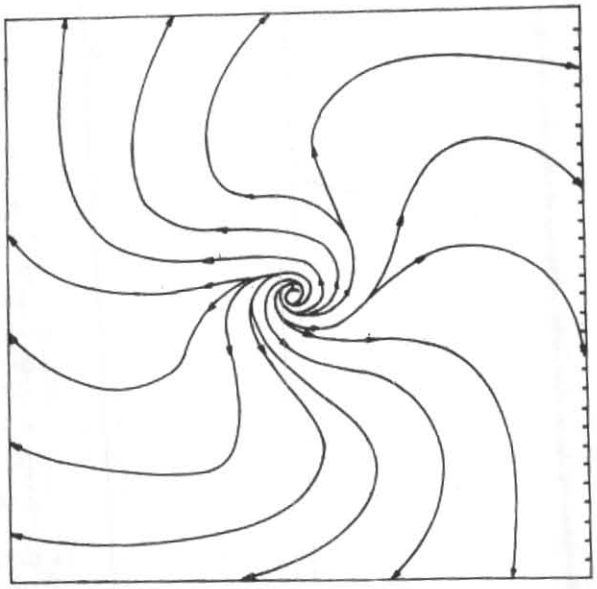

Fig. 9. Streamlines (A) of upper level at 48-hour, 18 km grid

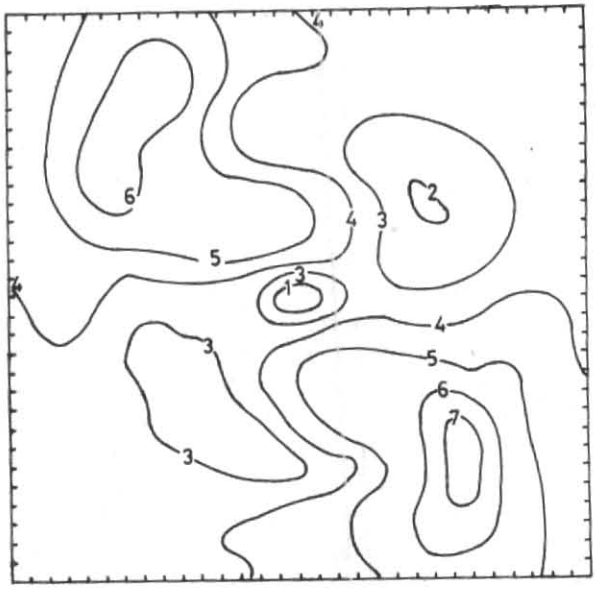

Fig. 10. Isotach (A) of upper level at 48-hour, 18 km grid. Units : Knots

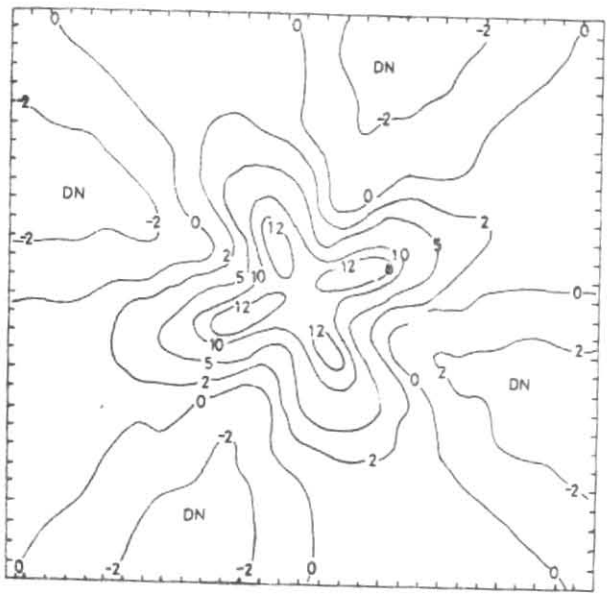

Fig. 11. Vertical motion (A) at 1.0 km (w_1) at 48-hour, Units : cm/sec, 18 km grid

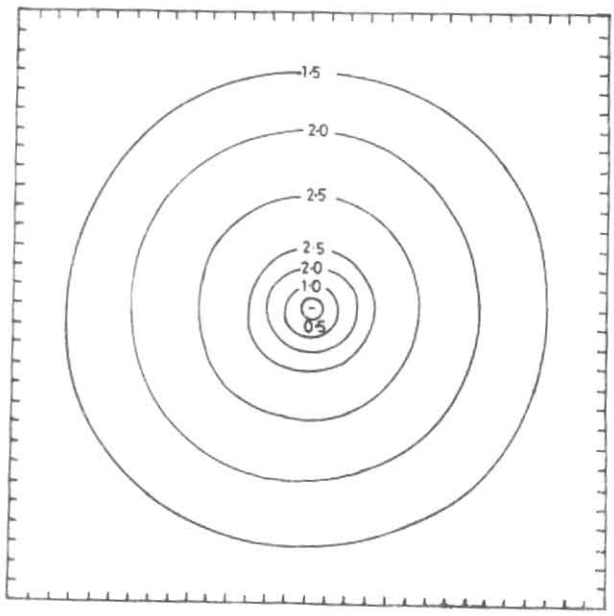

Fig. 12. Air temperature anomaly (A) at upper level at 48 hour. Unit: °C

(Fig. 9), cyclonic inside a radius of 100 km and anticyclonic outside. But, middle level wind directions (Fig. 8) indicate practically no inflow or outflow. The centre of the flow pattern at each level lies on the centre of the vortex on the surface. This is expected as the vortex was not allowed to interact with other system. The isotach analysis on the surface indicates that the wind speed is also nearly symmetric about the centre. The inner pressure profiles are nearly circular, and on the surface they are closely packed. Outer profiles indicate that matching of the solutions between grids of different lengths did not produce any unwanted effect. There is a noticeable asymmetry of the isotach field in the upper level (Fig. 10) with higher wind speed to the northwest and southeast sectors.

The vertical velocity w_1 at the top of the boundary layer at 48-hour in A is shown in Fig. 11. It increased slowly with time and region of high speed gradually moved towards the centre. At 48-hour, it reached to 13 to 15 cm/sec in an annular region between 36 and 50 km from the centre. One interesting feature of w_1 is that band-like regions of upward motion are separated by descending motion. In the upper level, w_2 (Fig. not shown) is mainly ascending around the centre (maximum 32 cm/sec) with weak descending motion at a large distance.

In case A, at 48-hour, warm core in the middle level is noticeable at this stage (Fig. not shown). The maximum positive potential temperature anomaly of 6°C, and air temperature (T) anomaly of 4.6°C, are located at the centre of the vortex. Both the anomaly profiles are nearly circular and concentric. Radial gradient of air temperature is highest around the centre; but that of potential temperature is highest between 36 and 54 km. The air temperature anomaly in the upper level is shown in Fig. 12. It is seen from the figure that the maximum warming at this level is not situated at the centre. It is negative only at the centre grid point and increases sharply with radius to more than 2.5°C, then decreases slowly outwards. Warming is maximum within an annular region approximately between 58 and 100 km around the centre. It's gradient is steep upto 60 km. Potential temperature anomaly (Fig. not shown) is negative in a very small area around the centre, and increases sharply with radius to more than 4.0°C, then decreases slowly outwards. This implies that warming in the central part of upper layer is not yet sufficient enough to compensate adiabatic cooling due to vertical motion in the centre.

At 24-hour, in the frictionless case (B) (Figs. not shown) alternate region of ascending and descending motion are observed at the top of the boundary layer. In the central region of about 90 km radius,

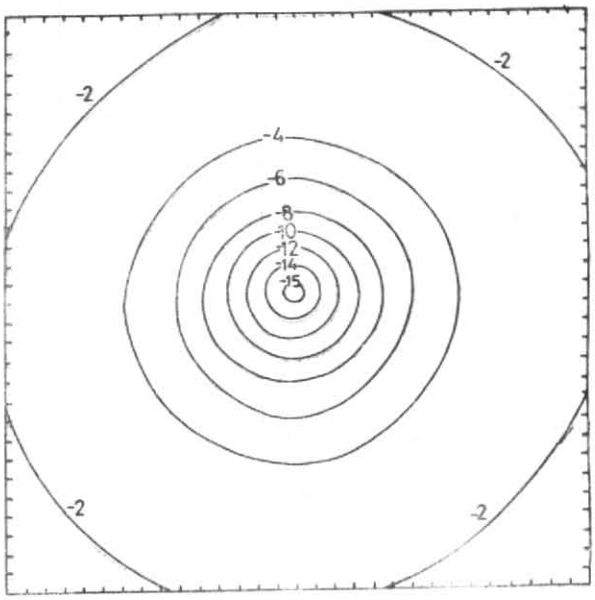

Fig. 13. Sea level pressure anomaly (B) at 60-hour, 18-km grid. Unit : hPa

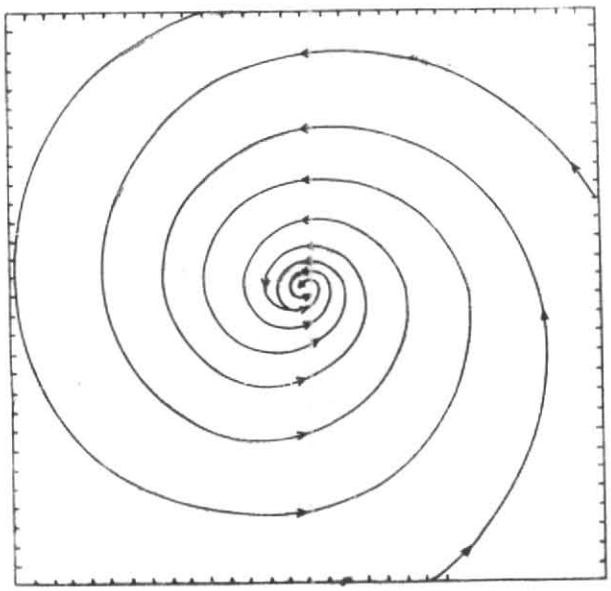

Fig. 14. Streamlines (B) of 0.5 km level at 60-hour, 18 km grid

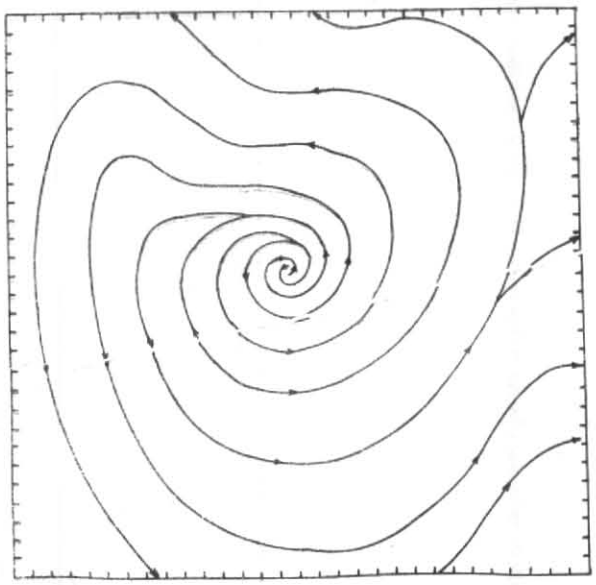

Fig. 15. Streamlines (B) of upper level at 60-hour, 18 km grid

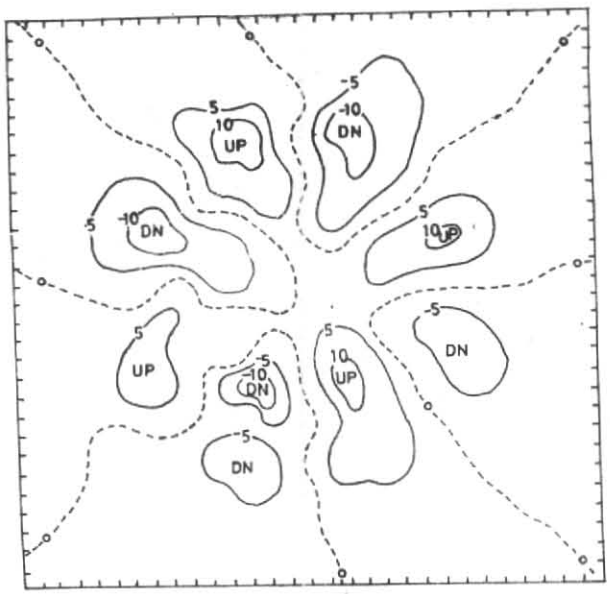

Fig. 16. Vertical motion (B) at 1.0 km (w_1) at 60-hour, Units : cm/sec, 18 km grid

the upward velocity is very small and almost all parts of the outer region are covered with sinking motion. At the upper level, the pattern is similar to that at lower level. This suggests that such patterns may be independent of friction and probably linked to the dynamics and thermodynamics of the flow itself. The potential temperature anomaly profiles at 24-hour are circular and symmetric. In the middle level, the anomaly is positive with its maximum at the centre (4°C). While in the upper level, it is negative (≈ -1°C) at the centre and weak positive at large distance.

Sea level pressure anomalies, streamlines at lower and upper levels and w_1 for this case at 60-hour are shown in Figs. 13 to 16. The pressure anomaly pattern in the inner domain represents circular contours comparable to observation. The streamlines in the boundary layer are symmetric. The angle of inflow is very small (1 to 3 degree). This could be expected as the surface friction and diffusion terms are excluded in this experiment. The streamlines and inflow angle in the middle level (not shown) are similar to those in the boundary layer. In the upper level these are not symmetric. A large area in the centre is dominated by cyclonic outflow which is surrounded by a trough and two weak ridges. Anthes (1972) concluded that the asymmetry of the outflow layer results from dynamic instability. This may also happen due to Cartesian co-ordinate being used for circularly symmetric system.

Due to increase of the potential temperature in the middle and upper layers, the pressure gradient force increased steadily during the later part of integration. This increased pressure gradient force accelerated the radial influx of mass in the lower layer. The major part of the radial momentum, thus created, was converted into the tangential momentum by Coriolis force, thereby increasing the tangential momentum to restore partly the gradient wind balance. In cases with friction, there was loss of tangential momentum to the ocean surface and gradient wind balance of the vortex was disturbed leaving to an unbalanced pressure gradient force directed to the centre. As a result, rings of air started to move toward the centre in the boundary layer and a part of which was also converted to tangential momentum. Thus, the radius of the maximum tangential velocity in the frictional cases (A and C) has been decreased. In frictionless case, this reduction is very less in comparison with frictional cases. With friction, the rate of increase of surface wind depends upon the excess of tangential momentum generated by heating over the loss due to surface friction and turbulent diffusions. Hence, the increase of tangential velocity is highest in B and lowest in C.

The cyclonic flow in the upper troposphere slowly disappeared and anticyclonic outflow formed and intensified with time. The air converging in the boundary layer rose and diverged out in the upper troposphere due to decrease of pressure gradient force. The absolute angular momentum of a parcel of air moving horizontally in the upper troposphere is nearly conserved; so the relative angular momentum of diverging air decreases with radius. Thus, the initial cyclonic circulation in the upper level weakened slowly and anticyclonic ouflow formed away from the axis. The vortex remained stationary and nearly symmetric during the period of integration in all cases, since it was not allowed to interact with other system of the atmosphere.

7. Summary and remarks

From the results of three cases tested in this preliminary study, it is clear that the staggered grid scheme, finite difference method, matching of solutions between meshes of different grid lengths and the technique of integration have yielded smooth and encouraging results. Therefore, we may conclude that the present scheme has shown satisfatory performance from the computational point of view. Using the new iterative method for solution of the system of Helmholtz equations developed in this study, the semi-implicit method has become more advantageous in speed for the nested grid model. In this regard, the purpose of the present experiment has been fulfilled.

The results of the numerical experiment indicate that a disturbance may develop without surface friction. It may be inferred that surface friction may not play an essential role in the early developing stage of a tropical storm when the vortex is weak, as the frictional convergence at this stage may not be sufficient for its growth. That is, the CISK mechanism may not be very relevant to pre-storm disturbance maintenance and intensification. On the other hand, initiation of initial development to the storm's intensity may be attributed to the warming caused by forced subsidence in the central region of the disturbance as postulated by several authors.

The structure of the disturbance obtained in frictionless case at 60-hour is different from the real storm in the sense that it has very less convergence in the boundary layer. The radius of the maximum tangential velocity is also much higher than the frictional case. This suggests that surface friction comes into play when the strength of the vortex is increased and it is one of the important factors to determine the scale of the disturbance.

An interesting related application of this work, for example, may be conducting experiments for tropical storm modification. Since, the behaviour of a storm may be examined adding heat directly or indirectly in the upper layers.

There are several deficiencies in the model. The heating due to forced subsidence has been incorporated through an analytic function. This is to be parametrized in terms of large scale flow. The vertical resolution of the model is poor. Heat transfer between ocean surface and the vortex has been formulated implicitly. Eddy coefficients of viscosity have been treated in a simple fashion. This model can be further extended and refined to study small scale weather phenomena and the life-cycle of a tropical storm taking into consideration the variation of Coriolis parameter, environmental flow with movable nested grids, more sophisticated parametrization of physical processes, smaller grid lengths etc., if high speed computer facility is available.

Acknowledgement

The author wishes to express his sincere thanks to Dr. Ambarish Ghosh, Professor, Indian Statistical Institute, Calcutta University, Calcutta, for his encouragement throughout this study. He takes this opportunity to record his deep sense of gratitude to Dr. N. Sen Roy, Director General of Meteorology, India Meteorological Department, New Delhi, who provided computer facility in N.I.C., while the author was posted at New Delhi. Thanks are also due to Shri P. K. Misra, DDGM, R.M.C. Calcutta, who kindly went through the manuscript.

APPENDIX A

Finite-difference of non-linear terms

The following finite-difference and average operators are defined on a uniform horizontal mesh of uniform grid length Δs, for a dependent variable β, as discrete values of independent variables $x = i\Delta s$, $y = j\,\Delta s$ $(\Delta s \equiv \Delta x \equiv \Delta y)$:

$$\begin{aligned}
\beta_x &\equiv \left(\beta_{i+\frac{1}{2},j} - \beta_{i-\frac{1}{2},j}\right)/\Delta s \\
\bar{\beta}^x &\equiv \left(\beta_{i+\frac{1}{2},j} + \beta_{i-\frac{1}{2},j}\right)/2 \\
\beta_y &\equiv \left(\beta_{i,j+\frac{1}{2}} - \beta_{i,j-\frac{1}{2}}\right)/\Delta s \\
\bar{\beta}^y &\equiv \left(\beta_{i,j+\frac{1}{2}} + \beta_{i,j-\frac{1}{2}}\right)/2
\end{aligned} \tag{A1}$$

In addition to these operators along the coordinate directions, we define similar operators along the diagonals of a grid square (Ookochi 1972):

$$\begin{aligned}
\delta_a\beta &\equiv \left(\beta_{i+\frac{1}{2},j+\frac{1}{2}} - \beta_{i+\frac{1}{2},j-\frac{1}{2}}\right)/\Delta s \\
\bar{\delta}^a\beta &\equiv \left(\beta_{i+\frac{1}{2},j+\frac{1}{2}} + \beta_{i-\frac{1}{2},j-\frac{1}{2}}\right)/2 \\
\delta_b\beta &\equiv \left(\beta_{i+\frac{1}{2},j-\frac{1}{2}} - \beta_{i-\frac{1}{2},j+\frac{1}{2}}\right)/\Delta s \\
\bar{\delta}^b\beta &\equiv \left(\beta_{i+\frac{1}{2},j-\frac{1}{2}} + \beta_{i-\frac{1}{2},j+\frac{1}{2}}\right)/2
\end{aligned} \tag{A2}$$

The factor $\sqrt{2}$ that naturally occurs in the denominator of $\delta_a\beta$ and $\delta_b\beta$ has been omitted above and combined with $\sqrt{2}$ that occurs when the diagonal component is expressed in terms of momentum components.

In terms of the above operators, the finite difference equations for non-linear terms in the first and second equations of motion and energy equation can be written in the following form:

$$\begin{aligned}
&\frac{\partial}{\partial x}(\bar{\rho}uu) + \frac{\partial}{\partial y}(\bar{\rho}uv) + \frac{\partial}{\partial z}(\bar{\rho}uw) \\
&= \frac{2}{3}\left[\bar{\rho}\delta_x(\bar{u}^x\,\bar{u}^x) + \bar{\rho}\delta_y(\bar{u}^y\,\bar{v}^x)\right] \\
&+ \frac{1}{6}\left[\bar{\rho}\delta_a(\bar{u}^{xy}\,\bar{u}^{xy}) + \bar{\rho}\delta_b(\bar{u}^{xy}\,\bar{u}^{xy})\right] \\
&+ \frac{1}{6}\left[\bar{\rho}\delta_a(\bar{u}^{xy}\,v) - \bar{\rho}\delta_b(\bar{u}^{xy}\,v)\right] \\
&+ \delta_z\left[\bar{\rho}\,\bar{u}^z\,\bar{w}^x\right]
\end{aligned} \tag{A3}$$

$$\begin{aligned}
&\frac{\partial}{\partial x}(\bar{\rho}uv) + \frac{\partial}{\partial y}(\bar{\rho}vv) + \frac{\partial}{\partial z}(\bar{\rho}vw) \\
&= \frac{2}{3}\left[\bar{\rho}\delta_x(\bar{u}^y\,\bar{v}^x) + \bar{\rho}\delta_y(\bar{w}^y\,\bar{v}^y)\right]
\end{aligned}$$

$$+\frac{1}{6}\left[\bar{\rho}\delta_a(\bar{v}^{xy}\bar{v}^{xy})-\bar{\rho}\delta_b(\bar{v}^{xy}\bar{v}^{xy})\right]$$

$$+\frac{1}{6}\left[\bar{\rho}\delta_a(u\bar{v}^{xy})+\bar{\rho}\delta_b(u\bar{v}^{xy})\right]$$

$$+\delta_z[\bar{\rho}\,\bar{v}^z\,\bar{w}^y] \qquad \text{(A4)}$$

$$\frac{\partial}{\partial x}(\bar{\rho}u\alpha)+\frac{\partial}{\partial y}(\bar{\rho}v\alpha)$$

$$=\frac{2}{3}\left[\bar{\rho}\delta_x(\bar{u}^{xy}\bar{\alpha}^x)+\bar{\rho}\delta_y(\bar{v}^{xy}\bar{\alpha}^y)\right]$$

$$+\frac{1}{6}\left[\bar{\rho}\delta_a(\bar{u}^y\bar{\alpha}^a)+\bar{\rho}\delta_b(\bar{u}^y\bar{\alpha}^b)\right]$$

$$+\frac{1}{6}\left[\bar{\rho}\delta_a(\bar{v}^x\bar{\alpha}^a)-\bar{\rho}\delta_b(\bar{v}^x\bar{\alpha}^b)\right] \qquad \text{(A5)}$$

APPENDIX B

Iterative method for solution of a system of Helmholtz equations

In iterative method, an initial guess of the solution is made and then progressively improved until an acceptable level of accuracy is reached.

To illustrate our Simultaneous Multi-level Relaxation (SMR) method, let us consider a rectangular region consists of a grid of equally spaced points. The values of the variable, ϕ for which the solutions to the system of Helmholtz equations are sought, are specified on the outermost boundaries. The equations in this study are of the following form :

$$\nabla_H^2\phi_{i,j,1}+a_{11}\phi_{i,j,1}+a_{12}\phi_{i,j,2}+a_{13}\phi_{i,j,3}=F_{i,j,1} \qquad \text{(B1)}$$

$$\nabla_H^2\phi_{i,j,2}+a_{21}\phi_{i,j,1}+a_{22}\phi_{i,j,2}+a_{23}\phi_{i,j,3}=F_{i,j,2} \qquad \text{(B2)}$$

$$\nabla_H^2\phi_{i,j,3}+a_{11}\phi_{i,j,1}+a_{12}\phi_{i,j,2}+a_{13}\phi_{i,j,3}=F_{i,j,3} \qquad \text{(B3)}$$

where, ∇_H^2 is the 5-point Laplace operator; a_{11}, $a_{12}, \ldots\ldots a_{33}$ are co-efficients and $F_{i,j,1}$, $F_{i,j,2}$ and $F_{i,j,3}$ are forcing functions.

In Sequential Relaxation (SR) or Sussive Over Relaxation method (SOR), the correction to estimate (or guess) value using residual is applied to each equation separately and independently of other equations. In our method (SMR) the residuals on a particular grid point '*i, j*' on all levels are calculated first as in SR method, and corrections to previous "guess values" at that particular horizontal grid point on all levels are done simultaneously taking into account each and every terms of all equations, rather than each level separately, since the change in one level affects other levels also.

Let $\phi^m_{i,j,k}$ represent the 'm'th estimate of $\phi_{i,j,k}$. Then the residuals $R^m_{i,j,k}$ $(k = 1, 3)$, for the 'm'th estimate is defined as follows :

$$R^m_{i,j,1}=\phi^{m+1}_{i-1,j,1}+\phi^m_{i+1,j,1}+\phi^{m+1}_{i,j-1,1}+\phi^m_{i,j+1,1}-4\,\phi^m_{i,j,1}+a_{11}\phi^m_{i,j,1}+a_{12}\phi^m_{i,j,2}+a_{13}\phi^m_{i,j,3}-F_{i,j,1} \qquad \text{(B4)}$$

Similarly, $R^m_{i,j,2}$ and $R^m_{i,j,3}$ are calculated.

If, $R^m_{i,j,1}$, $R^m_{i,j,2}$ and $R^m_{i,j,3}$ just happened to vanish at all points, then $\phi^m_{i,j,1}$, $\phi^m_{i,j,2}$ and $\phi^m_{i,j,3}$ would be the true solutions of the equations (B1) to (B3).

Let us now suppose that our guesses at the particular point '*i, j*' on all three levels were changed by amounts $\delta\phi_{i,j,1}$, $\delta\phi_{i,j,2}$ and $\delta\phi_{i,j,3}$ respectively, without altering the guess at any of the surrounding points. Since the forcing functions are fixed, the equation (B4) implies that the resulting changes in ϕ's will make residuals of all equations to zero, if the following relations are satisfied.

$$(-4+a_{11})\delta\phi_{i,j,1}+a_{12}\delta\phi_{i,j,2}+a_{13}\delta\phi_{i,j,3}=-R_{i,j,1} \qquad \text{(B5)}$$

$$a_{21}\delta\phi_{i,j,1}+(-4+a_{22})\delta\phi_{i,j,2}+a_{23}\delta\phi_{i,j,3}=-R_{i,j,2} \qquad \text{(B6)}$$

$$a_{31}\delta\phi_{i,j,1}+a_{32}\delta\phi_{i,j,2}+(-4+a_{33})\delta\phi_{i,j,3}=-R_{i,j,3} \qquad \text{(B7)}$$

Above three algebraic equations can be easily solved for $\delta\phi_{i,j,1}$, $\delta\phi_{i,j,2}$ and $\delta\phi_{i,j,3}$ and $(m+1)$th guess can be obtained from the following relations :

$$\phi^{m+1}_{i,j,1} = \phi^{m}_{i,j,1} + \delta\phi_{i,j,1}$$

$$\phi^{m+1}_{i,j,2} = \phi^{m}_{i,j,2} + \delta\phi_{i,j,2} \qquad \text{(B8)}$$

$$\phi^{m+1}_{i,j,3} = \phi^{m}_{i,j,3} + \delta\phi_{i,j,3}$$

This procedure is applied to all internal grid points and iterations are repeated and the solutions progressively improved until the maximum of the absolute value of residual becomes less than an optimum value.

References

Anthes, R. A., 1972, "Development of asymmetries in the three dimensional model of the tropical cyclone", *Mon. Weath. Rev.*, **100**, 461-476.

Arnold, C. P., 1977, "Tropical cyclone cloud and intensity relationships", Colo. State Univ., paper No. 277, pp. 154.

Browning, G., Kesiss, H. and Oliger, J., 1973, "Mesh refinement", *Math. Comp.*, **27**, 29-39.

Chen, J. H. and Miyakoda, K., 1974, "A nested grid computation for the barotropic free surface atmosphere", *Mon. Weath. Rev.*, **102**, 181-190.

Elsberry, R. L., 1979, "Applications of tropical cyclone models", *Bull. Amer. Met. Soc.*, **60**, 750-762.

Francis, P.E., 1975, "Use of a multipoint filter as a dissipative mechanism in a numerical model of the general circulation of the atmosphere", *Quart. J. R. Met. Soc.*, **101**, 567-582.

Frank, W. M., 1977, "The structure and energetics of the tropical cyclone, I-Storm structure", *Mon. Weath. Rev.*, **105**, 1119-1135.

Grammeltvedt, A., 1969, "A survey of finite-difference schemes for the primitive equations for barotropic fluid", *Mon. Weath. Rev.*, **97**, 384-404.

Gray, W. M., 1977, "Tropical disurbance to cyclone intensification", Paper presented at the 11th Tech. Conf. of Hurricane and Tropical Meteorology, Miami, Florida.

Gray, W. M., 1979, "Hurricanes : Their formation, structure and likely role in the tropical circulation. Meteorology over the tropical oceans", Ed. *Roy. Meteor. Soc.*, 155-218.

Harrison, E. J., 1973, "Three-dimensional numerical simulations of tropical systems utilizing nested finite grids", *J. Atmos. Sci.*, **30**, 1528-1543.

Hawkins, H. F. and Rubsam, D. T., 1968, "Hurricane 'Hilda' 1964 : II. Structure and budgets of the hurricane on October, 1964", *Mon. Weath. Rev.*, **96**, 617-636.

Hill, G. E., 1968, "Grid telescopic in numerical weather prediction", *J. Appl. Meteor.*, **7**, 29-38.

Jones, R. W., 1977, "A nested grid for a three-dimensional model of tropical cyclone", *J. Atoms. Sci.*, **34**, 1528-1543.

Kwizak, M. and Robert, A. J., 1971, "A semi-implicit scheme for grid point atmospheric models of the primitive equations", *Mon. Weath. Rev.*, **99**, 32-36.

Ley, G. W., and Elsberry, R. L., 1976, "Forecasts of typhoon Irma using nested grid model", *Mon. Weath. Rev.*, **104**, 1154-1161.

Madala, R. V. and Piacsek, S. A., 1975, "Numerical simulation of asymmetric hurricanes on a β-plane with vertical shear", *Tellus*, XXVII, **5**, 453-468.

Madala, R. V., 1978, "An efficient direct solver for separable and non-separable Elliptic equations", *Mon. Weath. Rev.*, **106**, 1735-1741.

Mandal, J. C., 1989, "Studies on some aspects of tropical storm and other vortices", Ph.D. dissertation, Calcutta University, Chap. IV, 107-187.

Mathur, M. B., 1974, "A multiple-grid primitive equation model to simulate the development of an asymmetric hurricane (Isbell 1964)", *J. Atmos. Sci.*, **31**, 371-393.

Matsuno, T., 1966, "Numerical integrations of the primitive equations by a suitable backward difference method", *J. Met. Soc. Japan, Ser.* 2, **44**, 76-84.

McGregor, J. L. and Leslie, L. M., 1977, "On the selection of grids for semi-implicit schemes", *Mon. Weath. Rev.*, **105**, 236-238.

Miller, B. I., 1962, "On the momentum and energy budget of hurricane Helene (1958)", Nat. Hurricane Res. Project Report No. 66.

Ogura, Y. and Charney, J. C., 1962, "A numerical model of thermal convection in the atmosphere", Numerical Weather Prediction, Tokyo, Japan, 431-452.

Ogura, Y. and Phillips, N. A., 1962, "Scale analysis of deep and shallow convection in the atmosphere", *J. Atmos. Sci.*, **19**, 173-179.

Ookochi, Y., 1972, "A computational scheme for the nesting fine mesh in the primitive equation model", *J. Meteor. Soc. Japan*, **50**, 37-47.

Ookochi, Y., 1978, "Preliminary test of typhoon forecast with a moving multi-nested grid", *J. Met. Soc. Japan*, **56**, 571-582.

Ooyama, K., 1969, "Numerical simulation of the life cycle of tropical cyclones, *J. Atmos. Sci.*, **26**, 3-40.

Palmen, E. H., 1948, "On the formation and structure of tropical hurricanes", *Geophysica*, **48**, 24-38.

Robert, A., Henderson, J. and Turnbull, C., 1972, "An implicit time integration scheme for baroclinic models of atmosphere", *Mon. Weath. Rev.*, **100**, 329-355.

Rosenthal, S. L., 1969, "Numeral experiments with a multilevel primitive equation model designed to simulate the development of tropical cyclones", Experiment I. Nat. Hurr. Res. Lab. Tech. Memo No. **82**, p. 36.

Sella, J. and Scolnik, S., 1972, "Method for solving simultaneous helmholtz equations", *Mon. Weath. Rev.*, **100**, 644-645.

Shuman, F. G., 1957, "Numerical methods in weather prediction. II smoothing and filtering", *Mon. Weath. Rev.*, **85**, 357-363.

Sturat, D. W., and O'Neill, T. H. R., 1967, "The over-relaxation factor in the numerical solution of the Omega equation", *Mon. Weath. Rev.*, **95**, 303-307.

Sundquvist, H., 1970, "Numerical simulation of the development of the tropical cyclones with ten level model", *Tellus*, Part I, **22**, 359-390.

Williams, G. P., 1969, "Numerical integration of the three dimensional Navier Stokes equations for incompressible flow", *J. Fluid Mech.*, **37**, 727-750.

Wu, J., 1969, "Wind stress and surface roughness at air-sea interface", *J. Geophys. Res.*, **74**, 444-459.

Yamasaki, M., 1968, "A tropical cyclone model with parameterized vertical partition of released latent heat", *J. Met. Soc. Japan*, **46**, 202-214.

Yamasaki, M., 1977, "The role of surface friction in tropical cyclones", *J. Met. Soc. Japan*, **55**, 559-571.

Yanai, M., 1961, "A detailed analysis of typhoon formation", *J. Meteor. Soc. Japan*, **39**, 187-214.